ACS APPLIED MATERIALS & INTERFACES

Research Article

www.acsami.org

Simultaneous Photodynamic and Photothermal Therapy Using Photosensitizer-Functionalized Pd Nanosheets by Single Continuous Wave Laser

Zengxia Zhao,[†] Saige Shi,[†] Yizhuan Huang,[†] Shaoheng Tang,[†] and Xiaolan Chen*[,†,‡]

[†]Department of Chemistry, College of Chemistry and Chemical Engineering, Xiamen University, Xiamen, 361005, P.R. China

[‡]State Key Laboratory of Chemo/Biosensing and Chemometrics, Hunan University, Changsha, 410082, P.R. China

Supporting Information

ABSTRACT: In this work, we prepared chlorin e6 (Ce6)-functionalized Pd nanosheets (Pd-PEI-Ce6) for the photodynamic and photothermal combined therapy that use a single laser. To fabricate the Pd-PEI-Ce6 nanocomposite, photosensitizer Ce6 were chemically conjugated to polyethylenimine (PEI) and the formed Ce6-PEI conjugates were then anchored onto Pd nanosheets by electrostatic and coordination interaction. The prepared Pd-PEI-Ce6 nanocomposite were about 4.5 nm in size, exhibited broad, and strong absorption from 450 to 800 nm, good singlet oxygen generation capacity and photothermal conversion efficiency, and excellent biocompability. Significantly greater cell killing was observed when HeLa cells incubated with Pd-PEI-Ce6 were irradiated with the 660 nm laser, attributable to both Pd nanosheets-mediated photothermal ablation and the photodynamic destruction effect of photosensitizer Ce6. The double phototherapy effect was also confirmed in vivo. It was found that the Pd-PEI-Ce6 treated tumor-bearing mice displayed the enhanced therapeutic efficiency compared to that of Pd-PEI, or Ce6-treated mice. Our work highlights the promise of using Pd nanosheets for potential multimode cancer therapies.

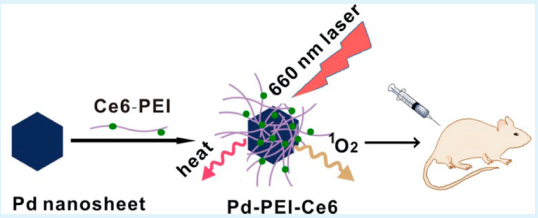

KEYWORDS: *Pd-PEI-Ce6 nanocomposite, photothermal therapy, photodynamic therapy, combinational therapy, in vivo*

1. INTRODUCTION

Photothermal therapy (PTT), which utilizes the electromagnetic radiation (most often in the form of infrared) to produce significant local hyperthermia for destruction of cells or tissues,[1] has recently emerged as a new candidate technique for cancer treatment. The photothermal conversion efficiency mainly relies on the kind of photothermal agents if the laser power is kept constant. Up to now, several types of photoabsorbing agents such as indocyanine green,[2,3] gold nanostructures,[4−9] carbon-based nanomaterials,[10−15] copper chalcogenide semiconductors,[16−20] Pd (palladium) nanosheets,[21,22] Bi_2Se_3 nanoplates[23] and $W_{18}O_{49}$ nanowires[24] have been developed for cancer PTT. However, the serious photobleaching of indocyanine green molecules under laser irradiation limits their wide applications. Although gold nanostructures are the most studied agents for the near-infrared (NIR) PTT, many anisotropic and hollow Au nanostructures lack of good photothermal stability upon irradiation of NIR laser, thereby inevitably imposing limitations in their practical therapeutic applications.[21,25−28] In comparison, the Pd-based species including Pd and Pd@Ag nanosheets et al., are new kind of promising photothermal agents because of their strong absorption in the near-infrared region, high photothermal conversion efficiency, excellent photothermal stability and biocompatibility.[21,22,25] More importantly, by changing the synthesis condition, a series of different sizes of Pd nanosheets with tunable NIR maximum absorption can be prepared. Recently, our group also has prepared ultrasmall Pd (palladium) nanosheets with the average diameter of ∼4.4 nm. These ultrasmall Pd nanosheets also exhibit high absorption in the NIR region, good biocompatibility and are easy to clear out of the body through renal excretion.[29]

Photodynamic therapy (PDT) is another light-based technique for cancer therapy by the generation of reactive oxygen species (ROS) including singlet oxygen.[30] However, the application of many photosensitizers (PSs) in clinic has been hindered by their limited tumor selectivity, hydrophobicity and easy aggregation in aqueous solution. For circumventing these drawbacks, various nanocarriers have been actively developed for effective delivery of PSs.[31]

To further improve therapeutic efficiency and obtain the best treatment effect, it is of great interest to develop combination therapy in which two or multiple treatment modes are effectively fell together and simultaneously treat cancer tissues. Compared with individual treatment method, combined treatment shows outstanding synergistic or collaborative effect, makes up the shortcoming of single treatment mode, therefore high therapeutic index can be achieved.

By loading photosensitizers on Au,[32−40] carbon,[14,41,42] Pd,[43] silica,[44] etc. nanostructures, researchers have fabricated some

Received: March 19, 2014
Accepted: May 6, 2014
Published: May 6, 2014

   dx.doi.org/10.1021/am501608c | ACS Appl. Mater. Interfaces 2014, 6, 8878−8885

successful nanocomposites for not only effective delivery of PSs but also combining PTT with PDT to eradicate cancer via synergistic effect. Unfortunately, as nanostructures and photosensitizers at NIR region have different maximum absorptions, it is difficult to use single wavelength laser for simultaneous PDT and PTT in most previous work.[32,33,38,39] Using two wavelength lasers for sequential exciting PDT and PTT will complicate the treatment process owing to the difficulty in the focus of the two laser beams at the same position.[34−36,41−43] Thus, the development of novel nanomaterials for combining PDT and PTT with high efficiency is highly desired.

In the present study, we have prepared a Pd-PEI-Ce6 nanocomposite by first modifying Chlorin e6 (Ce6) with polyethylenimine (PEI) (Ce6-PEI) and then loading the Ce6-PEI conjugate onto the small Pd nanosheets. The Ce6 and Pd nanosheets functioned as the PDT and PTT agents, respectively, and PEI was used to improve the water-solubility of the system in aqueous solution as well as act as the linker between Ce6 and Pd nanosheets. The fabricated Pd-PEI-Ce6 nanocomposite exhibited the following advantages: (i) Since both small Pd nanosheets and Ce6 have strong and matched maximum absorptions at about 660 nm in the 600 to 800 nm NIR phototherapeutic window, 660 nm single continuous wave (CW) laser was employed to excite PDT and PTT simultaneously, which will greatly simplify the experimental process and enhance the therapeutic efficiency. (ii) Their sizes are small (~4.5 nm) and display good singlet oxygen generation capacity, photothermal conversion efficiency and excellent biocompability, which will benefit the in vivo treatment application. (iii) The lower 660 nm laser power density used (0.5 W/cm^2) can protect photosensitizer Ce6 from photobleaching by laser irradiation. We found that the PDT/PTT double therapy using Pd-PEI-Ce6 had greater anticancer effects than either PDT using Ce6 or PTT using Pd nanosheets. Remarkably, when the Pd-PEI-Ce6 was injected into tumors that were subcutaneously transplanted into mice and after laser-irradiated, the tumors will be cured completely in the next 7days.

2. MATERIALS AND METHODS

2.1. Materials. Palladium(II) acetylacetonate ($Pd(acac)_2$), *N*,*N*-dimethylpropionamide (DMP), *N*-hydroxysuccinimide (NHS), 1-ethyl-3-[3-(dimethylamino)propyl]carbodiimide hydrochloride (EDC), polyethylenimine (PEI, M_n = 60000), and methylthiazolyldiphenyl-tetrazolium bromide (MTT) were purchased from Sigma-Aldrich. Chlorin e6 (Ce6) was ordered from the Frontier Scientific Inc., U.S.A. All chemicals were obtained from commercial supplies and used without further purification.

2.2. Preparation of Small Pd Nanosheets. Ten milligrams of $Pd(acac)_2$, 32 mg of poly(vinylpyrrolidone) (PVP, MW = 30000), and 30.6 mg of NaBr were dissolved in 2 mL of DMP, and then 4 mL water was added to the mixture. After it was kept at room temperature overnight, the resulting homogeneous yellow solution was transferred to a glass pressure vessel. The vessel was then charged with CO to 1 bar and heated at 100 °C for 2.0 h. The obtained dark blue products were precipitated by acetone, further purified by an ethanol−acetone mixture, and finally stored at 4 °C for future use.

2.3. Synthesis of Ce6-PEI Conjugate. The Ce6-PEI conjugate was synthesized using a modification of the standard EDC−NHS reaction. Typically, 10 mg of Ce6 was dissolved in 0.5 mL of dimethyl sulfoxide (DMSO), followed by the addition of 20 mg of EDC, and 20 mg of NHS to activate for 4.5 h. Then 1 mg of PEI aqueous solution (1 mL) was added to the above activated solution, and the mixture was allowed to react at room temperature for 12 h. The unreacted Ce6 and other chemicals were removed by ultrafiltration. The products were dispersed in ultrapure water for further characterization and application.

2.4. Preparation of Pd-PEI-Ce6 Nanocomposite. Five microliters of PEI-Ce6 conjugate was added to 200 μL of small Pd nanosheets dispersed in distilled water and the mixture was stirred overnight. The resultants were centrifuged by adding acetone and washed three times with ethanol. The products were dispersed in phosphate buffered solution (PBS) (pH = 7.4).

The content of Ce6 on the Pd nanosheets was determined indirectly by measuring the amount of unconjugated Ce6 in the supernatant using Ce6 UV−vis calibration curve at 658 nm after centrifuging the reaction solution (Figure S1, Supporting Information).

2.5. Singlet Oxygen Generation of Pd-PEI-Ce6. Singlet oxygen ($^1O_2$) generation of Pd-PEI-Ce6 was determined by using 1,3-diphenylisobenzofuran (DPBF) as a chemical $^1O_2$ probe, which reacts irreversibly with $^1O_2$ to cause a decrease in the DPBF absorption at about 400 nm. Briefly, 30 μL of DPBF (1.5 mg/mL in acetonitrile) was added to a solution of Pd-PEI-Ce6 in acetonitrile (2 mL, 50 μg/mL in Pd nanosheets). The solution was then irradiated with a 660 nm CW laser at the power density of 0.01 W/cm^2 for different periods of time, and the absorbance of DPBF at 410 nm was measured. Free Ce6 and Pd nanosheets in acetonitrile mixed with DPBF were introduced as control experiments.

2.6. Photothermal Effect Measurement. The photothermal conversion effect induced by the Pd-PEI-Ce6 was investigated by irradiating the Pd-PEI-Ce6 aqueous solution (1 mL) with a 660 nm laser (0.5 W/cm^2). The temperature of the solution was monitored using a submerged thermocouple microprobe.

2.7. Cell Culture. Human HeLa cell line was cultured in RPMI-1640 culture medium supplemented with 10% calf serum, 1% penicillin and 1% streptomycin. Cells were maintained at 37 °C in a humidified atmosphere containing 5% CO_2.

2.8. Cytotoxicity of Pd-PEI-Ce6. MTT assay was carried out to evaluate the potential cytotoxicity of Pd-PEI-Ce6 in cells. HeLa cells were seeded to 96-well plates at a density of 1 × 10^4 cells per well. Following cultivation for 12 h, cells were exposed to various concentrations of Pd-PEI-Ce6 (0, 5, 10, 25, 50, 100, 200 μg/mL) for 12, 24 and 48 h, respectively. A stock solution of MTT (25 μL, 5 mg/mL) was added into each well. After 4 h incubation at 37 °C, the MTT solution was replaced with 150 μL DMSO in each well. The plates were gently shaken for 20 min at room temperature before measuring the absorbance at 490 nm. All test samples were assayed in quintuplicate and the cell viability was calculated using the following formula: Cell viability = (mean absorbance of test wells − mean absorbance of medium control wells)/(mean absorbance of untreated wells − mean absorbance of medium control well) × 100%.

2.9. Cellular Uptake and Intracellular ROS generation of Pd-PEI-Ce6. HeLa cells were cultured in confocal dishes (35 mm) at a density of about 1 × 10^5 cells per dish for 12 h. Pd-PEI-Ce6 (50 μg/mL) was added to the dish and the cells were incubated for different periods of time at 37 °C. Afterward, the cells were washed three times with PBS and their nucleic were stained with 4′,6′-diamidino-2-phenylindole (DAPI) solution (5 μg/mL). Cell imaging of HeLa cells was performed by an Olympus FV-1000 laser confocal scanning microscope. The fluorescence emission of Ce6 was collected under 405 nm laser excitation.

The intracellular ROS generation was monitored by Reactive Oxygen Species Assay Kit based on DCFH-DA (2,7-dichlorodihydrofluorescein diacetate). HeLa cells were incubated with Pd-PEI-Ce6 for 4 h at 37 °C with 5% CO_2. After it was washed with PBS for 4 times, proper amount of DCFH-DA was added and irradiated with a 660 nm laser for 3 min, and 20 min later, the fluorescence images were taken by the confocal scanning microscope.

2.10. In Vitro PDT/PTT Combined Effects Induced by 660 nm CW Laser. HeLa cells were seeded onto 96-well plates with a density of 1 × 10^5 cells per well and incubated for 12 h. After cell attachment, Pd-PEI-Ce6 (containing 50 μg/mL Pd nanosheets), Pd-PEI (50 μg/mL), and Ce6 (2.77 μg/mL) were added to the wells and continued to culture for 12 h. After they were washed three times with PBS, the cells

in each well were exposed to 660 nm laser (0.5 W/cm^2) for 5 min. After staining with propidium iodide reagent (PI, 10 μg/mL), the cell fluorescence (Ex = 488 nm) was then assessed using the confocal fluorescent microscope. To quantitatively measure the number of HeLa cells that survived before and after irradiation, the cell viability was also measured by MTT assay as described above.

2.11. In Vivo PDT/PTT Combined Effects Induced by 660 nm CW Laser. The PDT/PTT combined anticancer effects of Pd-PEI-Ce6 in vivo were tested using S180-bearing mice. All animals were maintained and used in accordance with the Animal Management Rules of the Ministry of Health of the People's Republic of China and the guidelines for the Care and Use of Laboratory Animals of China. Female Kunming mice (~20 g provided from Laboratory Animal Center of Xiamen University) were subcutaneously injected S180 cells (~2 × 10^6) into the right rear legs in the mice. When the tumors reached about 70 mm^3 in volume, the mice were intratumorally injected with 80 μL of Pd-PEI-Ce6 (corresponding to 50 μg/mL Pd and 2.77 μg/mL Ce6). For control groups, mice were treated with the same volume of Pd-PEI (50 μg/mL), free Ce6 (2.77 μg/mL), and PBS, respectively. The tumors were irradiated with the 660 nm CW laser at a power density of 0.5 W/cm^2 for 5 min. During the laser irradiation, real-time temperature change of tumor surface was monitored by an infrared thermography (HM-300, Guangzhou SAT Infrared Technology Co., Ltd.). After treatment, the tumor sizes were measured by a caliper every 2 days, and the tumor volume was calculated as length × (width)^2 × 1/2. Relative tumor volumes were calculated as V/V_0 (V_0 and V stand for the tumor volume on the initial day and on the day of measurement, respectively).

3. RESULTS AND DISCUSSION

3.1. Synthesis and Characterization of the Pd-PEI-Ce6 Nanocomposite. The synthetic procedure for the Pd-PEI-Ce6 nanocomposite is represented in Scheme 1. Chlorin e6 (Ce6) is a widely used photosensitizer for experimental photodynamic therapy with limited water solubility. To improve its water-solubility, as well as effectively anchor onto the Pd nanosheets, the Ce6 was first conjugated with branched polyetheneimine (PEI), a hydrophilic polymer with abundant primary, secondary and tertiary amino groups, via amidation between the carboxyl group of Ce6 and the amino group of PEI in the presence of NHS and EDC as coupling agents (Scheme 1). The formation of Ce6-PEI conjugate was evidenced by zeta potential, Fourier transform infrared spectroscopy (FTIR) and UV−vis measurements (Figure 1a−c). Free Ce6 showed a zeta potential at −24.4 mV, which changed to +31.3 mV after PEI modification (Figure 1a). As demonstrated in Figure 1b, compared with the spectrum of pure PEI, in the FTIR of Ce6-PEI, the absorption at ~1650 cm^{-1} became stronger because of the formation of amido bond between Ce6 and PEI molecules. In addition, an obvious absorption peak at about 2900 cm^{-1} occurs, corresponding to the CH_2 stretching vibration of the PEI in the Ce6-PEI conjugate. From the absorption spectra, Ce6-PEI conjugate shows the similar characteristic absorption peaks as free Ce6 with Q-band at 658 nm (Figure 1c). These results suggested that Ce6 was successfully modified with PEI. The synthesized Ce6-PEI conjugate exhibited excellent water solubility, forming a transparent light green solution in phosphate buffered saline (2 in Figure 1d). Then the Ce6-PEI conjugate was anchored onto small Pd nanosheets by both electrostatic interaction between the positive charge Ce6-PEI and negative charge Pd nanosheets as well as coordination between Pd and the free NH_2 of Ce6-PEI conjugate. Transmission electron microscopy (TEM) measurements show that the prepared Pd-PEI-Ce6 are similar to the starting

Scheme 1. Preparation and Phototherapy Applications of Pd-PEI-Ce6 Nanocomposite

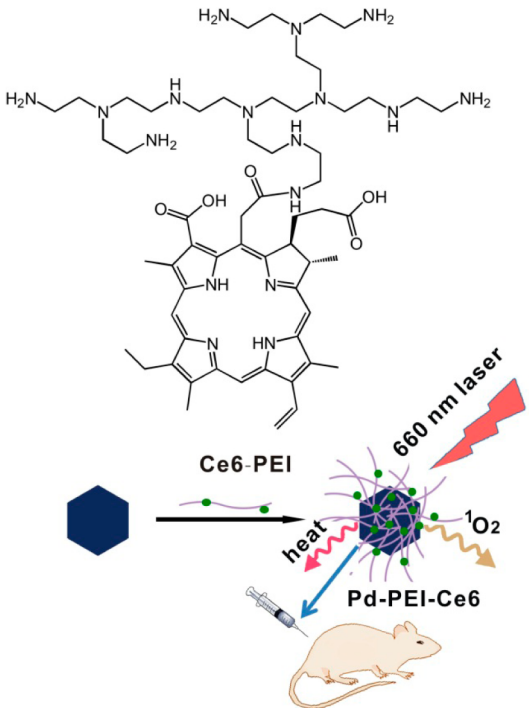

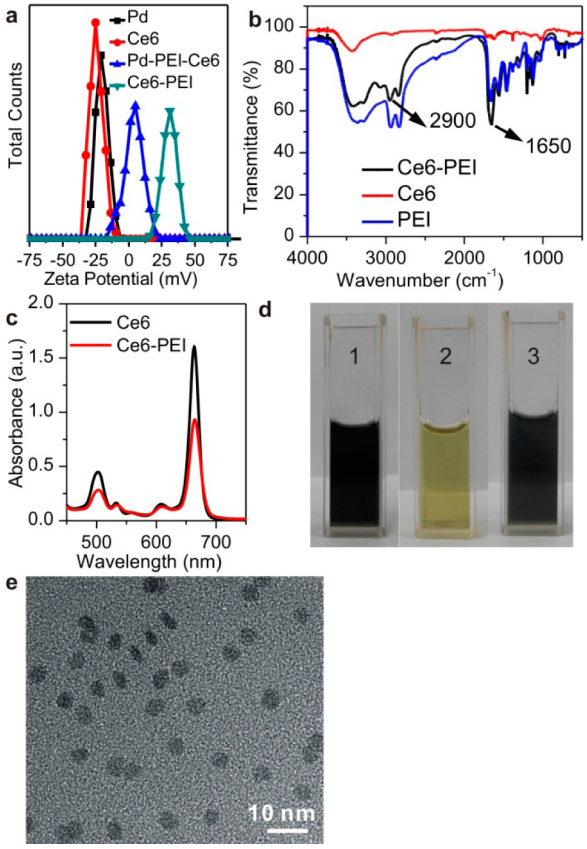

Figure 1. (a) ζ Potential distributions of Ce6, Ce6-PEI, Pd nanosheets, and Pd-PEI-Ce6 in water. (b) FTIR spectra of Ce6, PEI, and Ce6-PEI. (c) UV−vis absorption spectra of Ce6 and Ce6-PEI in PBS. (d) Photographs of Pd nanosheets (1), Ce6-PEI (2), and Pd-PEI-Ce6 (3) in PBS (pH = 7.4). (e) TEM images of Pd-PEI-Ce6.

dx.doi.org/10.1021/am501608c | ACS Appl. Mater. Interfaces 2014, 6, 8878−8885

Pd nanosheets (data not shown) with a mean diameter of about 4.5 nm (Figure 1e), indicating that the surface modification with Ce6-PEI did not significantly change the size and shape of Pd nanosheets. The Pd-PEI-Ce6 nanocomposite demonstrated very stable in different physiological solutions. No significant spectra changes have been observed for the nanocomposite stored in these solutions for 6 h (Figure S2, Supporting Information). In addition, after PEI-Ce6 conjugated with Pd nanosheets, the Pd-PEI-Ce6 had a zeta potential between the values of Ce6-PEI and Pd nanosheets, suggesting that Ce6-PEI conjugates were successful anchored on Pd nanosheets.

3.2. Photophysical and Photochemical Properties of Pd-PEI-Ce6 Nanocomposite. The small Pd nanosheets exhibit a strong absorption in the range of 450−800 nm with the maximum peak located at about 660 nm (Figure 2a). After the Ce6-PEI conjugate was loaded, the UV−vis spectrum of Pd-PEI-Ce6 showed the characteristics of both Pd nanosheets and Ce6. Besides the obvious wide absorption of Pd nanosheets, the characteristic Ce6 absorption peaks at 658 and 500 nm appear. The consistent maximum absorptions of Pd nanosheets and Ce6 in Pd-PEI-Ce6 nanocomposite implied that single wavelength laser, that is, 660 nm, can be used to irradiate them for both PTT and PDT. Moreover, according to the standard absorption curve of Ce6 at 658 nm, the loading amount of Ce6 onto Pd nanosheets was determined to be 5.25% (Figure S1, Supporting Information).

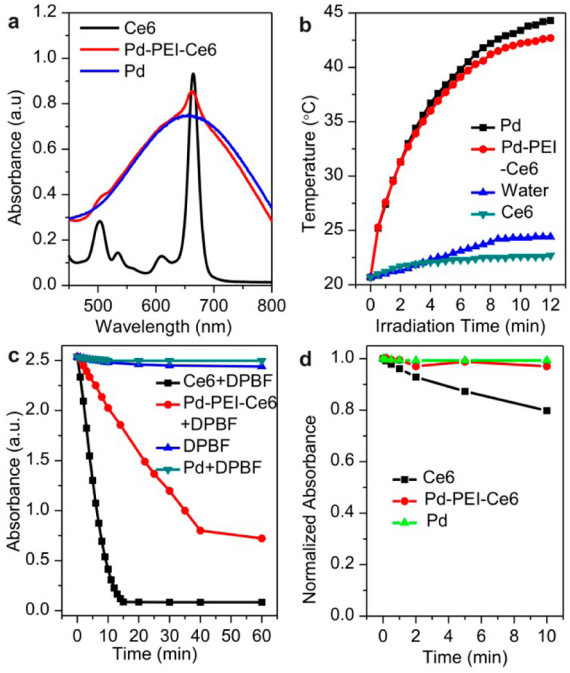

Figure 2. (a) UV−vis absorption spectra of Ce6, Pd-PEI-Ce6, and Pd nanosheets. (b) Temperature versus time plots of Pd nanosheets (50 μg/mL), Pd-PEI-Ce6 (50 μg/mL Pd and 2.77 μg/mL Ce6), Ce6 (2.77 μg/mL), and water under 660 nm laser irradiation at 0.5 W/cm^2. (c) Decay curves of DPBF absorption at 410 nm in different solutions as a function of irradiation time of 660 nm laser at 0.01 W/cm^2. (d) Normalized absorbance of Ce6, Pd-PEI-Ce6 and Pd nanosheets at 658 nm after different time of irradiation (660 nm, 0.5 W/cm^2).

Next, the photothermal conversion effect of Pd-PEI-Ce6 nanocomposite under the irradiation of 660 nm continuous wave laser was investigated. Both Pd nanosheets and Pd-PEI-Ce6 solutions with the same Pd amounts were exposed to the 660 nm laser at a power density of 0.5 W/cm^2 for 12 min, then the temperature changes were recorded. As presented in Figure 2b, similar temperature increases were observed for both small Pd nanosheets (~24 °C) and Pd-PEI-Ce6 (~22 °C), whereas free Ce6 solution or pure water exhibited a negligible change. These data confirm that the Pd-PEI-Ce6 nanocomposite could rapidly and efficiently convert the 660 nm laser energy into thermal energy.

The singlet oxygen ($^1O_2$) generation capability of Pd-PEI-Ce6 upon 660 nm laser irradiation was assessed by monitoring the time-dependent photodegradation of diphenylisobenzofuran (DPBF), a widely used singlet oxygen capture (Figure 2c). In the presence of Pd-PEI-Ce6 (containing 50 μg/mL Pd nanosheets and 2.77 μg/mL Ce6), the DPBF absorption at 410 nm significantly decreased when exposed to the 660 nm laser at a power density of 0.01W/cm^2, suggesting the efficient generation of $^1O_2$ by Pd-PEI-Ce6, although the $^1O_2$ production ability by Pd-PEI-Ce6 was weaker than that of free Ce6 owing to the irradiation light absorbed partly by the carrier Pd nanosheets.

In addition, the photostability of Pd nanosheets, free Ce6, and Pd-PEI-Ce6 after 660 nm laser irradiation for different periods was also investigated. It was found that after 5 min laser exposure at 0.5 W/cm^2, the absorption values of free Ce6 and Pd-PEI-Ce6 at 658 nm decreased about 15% and 7%, respectively, while the absorption of Pd nanosheets almost unchanged (0.7% of decrease), indicating the irradiation energy generated by the lower 660 nm laser power density (0.5 W/cm^2) caused little photobleaching to the Ce6 (Figure 2d and Figure S3, Supporting Information).

Taken together, Pd-PEI-Ce6 nanocomposite with outstanding properties, such as excellent photothermal conversion effect, high singlet oxygen generation capability and good photostability upon 660 nm CW laser irradiation, make them a promising candidate for application in PTT/PDT combined treatment.

3.3. In Vitro Cytotoxicity and Cellular Uptake of Pd-PEI-Ce6 Nanocomposite. Before the in vitro PDT/PTT combined therapy in cells, we first performed standard MTT assay to examine the cytotoxicity of the designed Pd-PEI-Ce6 nanocomposite. Different amounts of Pd-PEI-Ce6 were added to wells containing HeLa cells. After incubation for 12, 24 and 48 h, respectively, the cell viability was quantified by using the methyl thiazolyl tetrazolium (MTT) assay. Encouragingly, it was found that Pd-PEI-Ce6, even at a high dose concentration of 200 μg/mL, exhibited no appreciable negative effect on the viability of cells after 24 h exposure. When the incubation time was extended to 48 h, the viability percentage was somewhat lower, but still kept above 75% (Figure 3a). Observation from microscopic images also indicated that the cells retain good morphology and biological activity (Figure 3b). The results suggest that Pd-PEI-Ce6 nanocomposite possess good biocompatibility.

To examine the cellular uptake of Pd-PEI-Ce6, HeLa cells were incubated with Pd-PEI-Ce6 at 37 °C for 2, 4, and 6 h, respectively. After they were washed with PBS several times, cell nuclei were stained with DAPI and fluorescence imaging was performed by confocal microscopy. As shown in Figure 3c-h, strong red fluorescence of Ce6 was observed inside the cells and the fluorescence increased over incubation time, indicating the efficient cellular uptake of Ce6 loaded nanoparticles. In addition, the uptake of nanoparticles by cells was also concentration-dependent (Figure S4, Supporting Information).

dx.doi.org/10.1021/am501608c | ACS Appl. Mater. Interfaces 2014, 6, 8878−8885

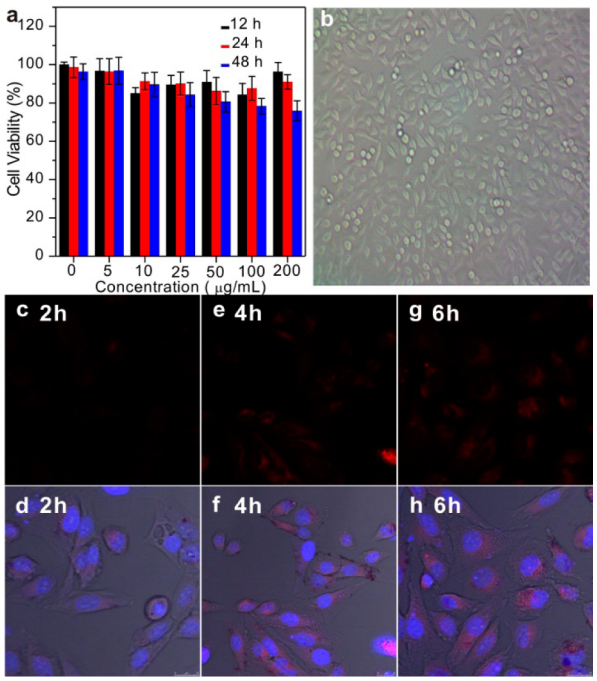

Figure 3. Cell cytotoxicity and cellar uptake of Pd-PEI-Ce6. (a) Cell viability of HeLa cells after incubation with increased concentration of Pd-PEI-Ce6 for 12, 24, and 48 h, respectively. (b) The cell morphology of HeLa cells incubated with 200 μg/mL Pd-PEI-Ce6 for 12 h. (c-h) HeLa cells incubated with Pd-PEI-Ce6 (containing 50 μg/mL Pd nanosheets and 2.77 μg/mL Ce6) for 2 (c and d), 4 (e and f), and 6 h (g and h), respectively.

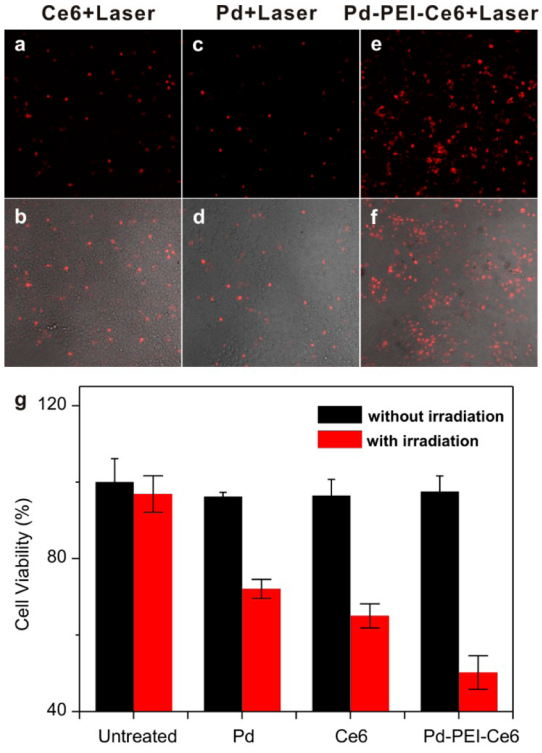

Figure 4. Fluorescence images of HeLa cells incubated with Ce6 (2.77 μg/mL, a and b), Pd-PEI nanosheets (50 μg/mL, c and d) and Pd-PEI-Ce6 (containing 50 μg/mL Pd nanosheets and 2.77 μg/mL Ce6, e and f) for 12 h with irradiation by a 660 nm CW laser at a power density of 0.5 W/cm^2 for 5 min. The cells were stained with propidium iodide (PI). (g) The corresponding cell viability after different treatments.

The higher concentration of nanoparticles, the more nanoparticles were taken up. The excellent cellular uptake of Pd-PEI-Ce6 is a benefit for the following phototherapy because the cells can easily be destroyed by both $^1O_2$ and heat produced from the nanoparticles. Furthermore, the outstanding fluorescent imaging properties of Pd-PEI-Ce6 also provide the possibility of imaging-tracking therapy.

3.4. In Vitro PDT/PTT Anticancer Effects of Pd-PEI-Ce6. As designed, the Pd-PEI-Ce6 nanocomposite will have PDT activity together with PTT ability upon 660 nm illumination. Since the lifetime of singlet oxygen is very short (e.g., 52 μs in acetonitrile solution and 3 μs in water),[45] if temperature increases, it might quench singlet oxygen and affect PDT efficiency. In our cell experiments, the production of ROS by Pd-PEI-Ce6 still can be observed after 3 min 660 nm laser irradiation at 0.5 W/cm^2 (Figure S5, Supporting Information), which imply that the temperature increase caused by the Pd nanosheets had little influence on the production of ROS.

We used the propidium iodide (PI), a nucleic acid dye which stains the dead cells, staining experiments to assess the viability of HeLa cells treated with the Pd-PEI-Ce6 upon laser irradiation. After incubation with Pd-PEI nanosheets, Pd-PEI-Ce6 or Ce6 for 12 h, the treated cells were then irradiated with a 660 nm laser at a power density of 0.5 W/cm^2 for 5 min. After staining the samples with PI following the standard protocol, microscopic images were performed and shown in Figure 4. More intense red fluorescence was observed from Pd-PEI-Ce6 treated cells than Ce6 or Pd nanosheets treated ones, which means that Pd-PEI-Ce6 kill more cells than either free Ce6 or Pd nanosheets alone after 5 min of irradiation.

The efficiency of the above materials killing HeLa cells was further analyzed by the MTT assay. As shown in Figure 4g, when the Pd-PEI-Ce6 (containing 50 μg/mL Pd nanosheets and 2.77 μg/mL Ce6) were incubated with the cancer cells and subsequently irradiated using the 660 nm laser at 0.5 W/cm^2 for 5 min, about 50% of the cells survived. While about 65% or 72% of HeLa cells survived when the cells were incubated with Pd-PEI (50 μg/mL) or Ce6 (2.77 μg/mL) alone after irradiation for 5 min. Moreover, in the absence of laser irradiation, no significant photodynamic or phototherapy anticancer effect was observed in any group. Also without any materials, the laser only did not cause any cytotoxicity. This further confirmed that the combined PDT and PTT multimodal nanoplatform based on Pd-PEI-Ce6 was a more efficient therapeutic protocol against cancer cells than either PDT or PTT alone.

3.5. In Vivo PDT/PTT Anticancer Effects of Pd-PEI-Ce6. The excellent in vitro phototherapeutic performance of Pd-PEI-Ce6 encouraged us to pursue their application in in vivo PDT/PTT combined therapy against kunming mice bearing S180 tumor. When the tumor volume grew to approximately 70 mm^3, the mice were randomly separated into four groups (five mice per group) and each tumor was injected a single time with 80 μL of PBS or 80 μL of a PBS dispersion of Ce6 (2.77 μg/mL), Pd-PEI (50 μg/mL Pd nanosheets), or Pd-PEI-Ce6 (containing 50 μg/mL Pd nanosheets and 2.77 μg/mL Ce6), respectively. After injection, the tumors were then exposed to a 660 nm laser at a power density of 0.5 W/cm^2 for 5 min. During the laser irradiation, full-body thermographic images

dx.doi.org/10.1021/am501608c | ACS Appl. Mater. Interfaces 2014, 6, 8878−8885

and the temperature profile (Figure 5) were recorded by an infrared camera. For the Pd-PEI nanosheets and Pd-PEI-Ce6

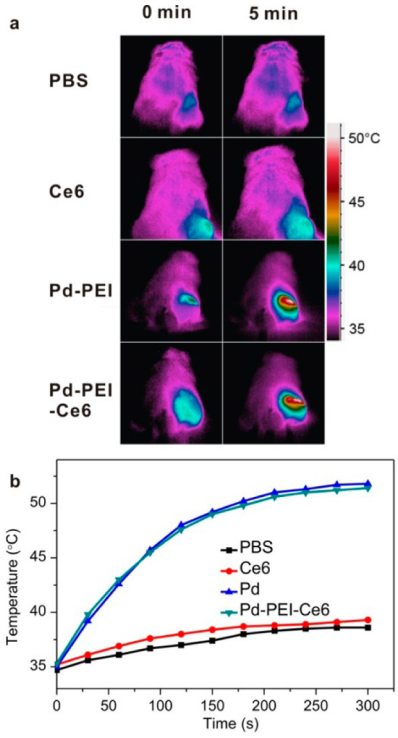

Figure 5. (a) IR thermal images of tumor-bearing mice with PBS, Ce6 (2.77 μg/mL), Pd-PEI (50 μg/mL Pd nanosheets), and Pd-PEI-Ce6 (containing 50 μg/mL Pd nanosheets and 2.77 μg/mL Ce6) injection exposed to the 660 nm laser at power densities of 0.5 W/cm^2 recorded at 0 and 5 min, respectively. (b) The corresponding temperature change of the tumor sites with irradiation by 660 nm laser (0.5 W/cm^2).

injected mice, the tumor temperature increased quickly from 35 to 52 °C after 5 min of laser exposure (Figure 5a). In comparison, only 4 °C temperature increase was observed for the saline or Ce6 injected mice. These results revealed that the Pd-PEI-Ce6 nanoparticles have the ability to induce hyperthermia by converting the 660 nm NIR light energy to heat in vivo.

The PDT/PTT phototherapeutic efficacy of Pd-PEI-Ce6 was further investigated. Tumor sizes are measured every 2 days after the above treatment and the relative tumor volume for each group is plotted as a function of time (the day in which the laser irradiation began was designated as day 1). As shown in Figure 6b, the mice treated with Ce6 (PDT alone) displayed slight decrease in tumor growth as compared to the PBS-treated mice, whereas the Pd-PEI treated mice (PTT alone) remarkably suppressed tumor growth during the initial 5 days and showed a slight growth after Day 5. In marked contrast, for the mice treated with both Pd-PEI-Ce6 and 660 nm laser, the solid tumor was rapidly reduced and completely eliminated from the mice after 7 days of treatment (Figure 6b). The corresponding photographs of the mice taken on day 1, day 3, and day 9 after different treatments are also presented in Figure 6a. These results demonstrated that PDT/PTT combined treatment using Pd-PEI-Ce6 was more effective in destroying tumors than PDT or PTT alone.

In addition, during this treatment period, neither obvious toxic side effect nor death was observed in all experimental

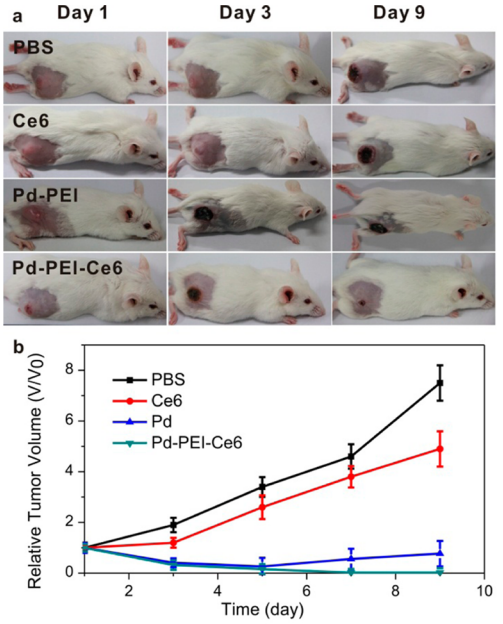

Figure 6. (a) Representative photographs of mice bearing S180 tumor after different treatments. (b) Growth of S180 tumors in different groups of mice after treatment. The relative tumor volumes were normalized to their initial sizes.

groups, implying that the Pd-PEI-Ce6 was not significantly toxic to the mice.

CONCLUSION

In summary, Pd-PEI-Ce6 nanocomposites have been successfully fabricated for near-infrared photodynamic and photothermal combination therapy of cancer both in vitro and in vivo. In the nanocomposite, Ce6 and Pd nanosheets served as the PDT and PTT agents, respectively, and PEI acted as the linker between Ce6 and Pd nanosheets. Since both small Pd nanosheets and Ce6 have strong and matched maximum absorptions in the 600 to 800 nm NIR phototherapeutic window, 660 nm single continuous wave (CW) laser with lower power density (0.5 W/cm^2) was employed to excite PDT and PTT simultaneously. In vitro cytotoxicity and in vivo antitumor efficiency examinations demonstrated the PDT/PTT double therapy using Pd-PEI-Ce6 had greater anticancer effects than either PDT using Ce6 or PTT using Pd nanosheets alone. This multifunctional therapeutic system should hold significant promise in the development of a new generation of cancer treatment systems.

ASSOCIATED CONTENT

Supporting Information

Further details of the UV−vis absorption spectra and linear curve of Ce6, UV−vis spectra of Pd-PEI-Ce6 dispersed in PBS and PBS with 10% FBS immediately and after 6 h, UV−vis absorption spectra changes of Ce6, Pd nanosheets and Pd-PEI-Ce6 nanocomposite after 660 nm laser irradiation at 0.5W/cm^2 for different time, confocal fluorescence image of HeLa cells incubated with Pd-PEI-Ce6 nanocomposite at different concentrations and confocal fluorescence images of HeLa cells to detect oxidative stress using Image-iT LIVE Reactive Oxygen Species (ROS) Kit. This material is available free of charge via the Internet at http://pubs.acs.org.

AUTHOR INFORMATION

Corresponding Author

*E-mail: chenxl@xmu.edu.cn.

Author Contributions

Z.X.Z. and S.G.S. contributed equally.

Notes

The authors declare no competing financial interest.

ACKNOWLEDGMENTS

We thank Professor Nanfeng Zheng for helpful discussions and comments on the manuscript. The work was supported by the National Natural Science Foundation of China (No.21101131), National Basic Research Foundation (973) of China (2014CB932004), Natural Science Foundation of Fujian Province (No.2012J01056), Fundamental Research Funds for the Central Universities (2010121015), and the open project grant from State Key Laboratory of Chemo/biosensing and Chemometrics (2013009).

REFERENCES

(1) Huang, N.; Wang, H.; Zhao, J.; Lui, H.; Korbelik, M.; Zeng, H. Single-Wall Carbon Nanotubes Assisted Photothermal Cancer Therapy: Animal Study with a Murine Model of Squamous Cell Carcinoma. *Lasers. Surg. Med.* **2010**, *42*, 638−648.

(2) Li, J.; Jiang, H.; Yu, Z.; Xia, H.; Zou, G.; Zhang, Q.; Yu, Y. Multifunctional Uniform Core−Shell Fe_3O_4@mSiO_2 Mesoporous Nanoparticles for Bimodal Imaging and Photothermal Therapy. *Chem.—Asian J.* **2013**, *8*, 385−391.

(3) Bardhan, R.; Chen, W.; Perez-Torres, C.; Bartels, M.; Huschka, R.; Zhao, L.; Morosan, E.; Pautler, R.; Joshi, A.; Halas, N. Nanoshells with Targeted Simultaneous Enhancement of Magnetic and Optical Imaging and Photothermal Therapeutic Response. *Adv. Funct. Mater.* **2009**, *19*, 3901−3909.

(4) Chen, B.; Meinertzhagen, I.; Shaw, S. Circadian Rhythms in Light-Evoked Responses of the Fly's Compound Eye, and the Effects of Neuromodulators 5-HT and the Peptide PDF. *J. Comp. Physiol. A* **1999**, *185*, 393−404.

(5) Hirsch, L.; Stafford, R.; Bankson, J.; Sershen, S.; Rivera, B.; Price, R.; Hazle, J.; Halas, N.; West, J. Nanoshell-Mediated Near-Infrared Thermal Therapy of Tumors under Magnetic Resonance Guidance. *Proc. Natl. Acad. Sci. U.S.A.* **2003**, *100*, 13549−13554.

(6) Wu, X.; Ming, T.; Wang, X.; Wang, P.; Wang, J.; Chen, J. High-Photoluminescence-Yield Gold Nanocubes: For Cell Imaging and Photothermal Therapy. *ACS Nano* **2010**, *4*, 113−120.

(7) Chen, J.; Glaus, C.; Laforest, R.; Zhang, Q.; Yang, M.; Gidding, M.; Welch, M. J.; Xia, Y. Gold Nanocages as Photothermal Transducers for Cancer Treatment. *Small* **2010**, *6*, 811−817.

(8) Chen, J.; Wang, D.; Xi, J.; Au, L.; Siekkinen, A.; Warsen, A.; Li, Z.-Y.; Zhang, H.; Xia, Y.; Li, X. Immuno Gold Nanocages with Tailored Optical Properties for Targeted Photothermal Destruction of Cancer Cells. *Nano Lett.* **2007**, *7*, 1318−1322.

(9) Park, H.; Yang, J.; Lee, J.; Haam, S.; Choi, I.-H.; Yoo, K.-H. Multifunctional Nanoparticles for Combined Doxorubicin and Photothermal Treatments. *ACS Nano* **2009**, *3*, 2919−2926.

(10) Wang, Y.; Fu, Y.; Peng, Q.; Guo, S.; Liu, G.; Li, J.; Yang, H.; Chen, G. Dye-Enhanced Graphene Oxide for Photothermal Therapy and Photoacoustic Imaging. *J. Mater. Chem. B* **2013**, *1*, 5762−5767.

(11) Kam, N.; O'Connell, M.; Wisdom, J.; Dai, H. Carbon Nanotubes as Multifunctional Biological Transporters and Near-Infrared Agents for Selective Cancer Cell Destruction. *Proc. Natl. Acad. Sci.U.S.A.* **2005**, *102*, 11600−11605.

(12) Chu, M.; Peng, J.; Zhao, J.; Liang, S.; Shao, Y.; Wu, Q. Laser Light Triggered-activated Carbon Nanosystem for Cancer Therapy. *Biomaterials* **2013**, *34*, 1820−1832.

(13) Yang, K.; Zhang, S.; Zhang, G.; Sun, X.; Lee, S. T.; Liu, Z. Graphene in Mice: Ultrahigh in Vivo Tumor Uptake and Efficient Photothermal Therapy. *Nano Lett.* **2010**, *10*, 3318−3323.

(14) Zhang, M.; Murakami, T.; Ajima, K.; Tsuchida, K.; Sandanayaka, A. S.; Ito, O.; Iijima, S.; Yudasaka, M. Fabrication of ZnPc/Protein Nanohorns for Double Photodynamic and Hyperthermic Cancer Phototherapy. *Proc. Natl. Acad. Sci. U.S.A.* **2008**, *105*, 14773−14778.

(15) Chakravarty, P.; Marches, R.; Zimmerman, N. S.; Swafford, A. D.; Bajaj, P.; Musselman, I. H.; Pantano, P.; Draper, R. K.; Vitetta, E. S. Thermal Ablation of Tumor Cells with Antibody-functionalized Single-walled Carbon Nanotubes. *Proc. Natl. Acad. Sci. U.S.A.* **2008**, *105*, 8697−8702.

(16) Li, Y.; Lu, W.; Huang, Q.; Li, C.; Chen, W. Copper Sulfide Nanoparticles for Photothermal Ablation of Tumor Cells. *Nanomedicine* **2010**, *5*, 1161−1171.

(17) Tian, Q.; Tang, M.; Sun, Y.; Zou, R.; Chen, Z.; Zhu, M.; Yang, S.; Wang, J.; Hu, J. Hydrophilic Flower-like CuS Superstructures as an Efficient 980 nm Laser-Driven Photothermal Agent for Ablation of Cancer Cells. *Adv. Mater.* **2011**, *23*, 3542−3547.

(18) Zhou, M.; Zhang, R.; Huang, M.; Lu, W.; Song, S.; Melancon, M. P.; Tian, M.; Liang, D.; Li, C. A Chelator-Free Multifunctional [64Cu]CuS Nanoparticle Platform for Simultaneous Micro-PET/CT Imaging and Photothermal Ablation Therapy. *J. Am. Chem. Soc.* **2010**, *132*, 15351−15358.

(19) Hessel, C.; Pattani, V.; Rasch, M.; Panthani, M.; Koo, B.; Tunnell, J.; Korgel, B. Copper Selenide Nanocrystals for Photothermal Therapy. *Nano Lett.* **2011**, *11*, 2560−2566.

(20) Yang, C.; Ma, L.; Zou, X.; Xiang, G.; Chen, W. Surface Plasmon-Enhanced Ag/CuS Nanocomposites for Cancer Treatment. *Cancer Nanotechnol.* **2013**, *4*, 81−89.

(21) Huang, X.; Tang, S.; Mu, X.; Dai, Y.; Chen, G.; Zhou, Z.; Ruan, F.; Yang, Z.; Zheng, N. Freestanding Palladium Nanosheets with Plasmonic and Catalytic Properties. *Nat. Nanotechnol.* **2011**, *6*, 28−32.

(22) Huang, X.; Tang, S.; Liu, B.; Ren, B.; Zheng, N. Enhancing the Photothermal Stability of Plasmonic Metal Nanoplates by a Core−Shell Architecture. *Adv. Mater.* **2011**, *23*, 3420−3425.

(23) Li, J.; Jiang, F.; Yang, B.; Song, X. R.; Liu, Y.; Yang, H. H.; Cao, D. R.; Shi, W. R.; Chen, G. N. Topological Insulator Bismuth Selenide as a Theranostic Platform for Simultaneous Cancer Imaging and Therapy. *Sci. Rep.* **2013**, DOI: 10.1038/srep01998.

(24) Kalluru, P.; Vankayala, R.; Chiang, C.-S.; Hwang, K. C. Photosensitization of Singlet Oxygen and in Vivo Photodynamic Therapeutic Effects Mediated by PEGylated $W_{18}O_{49}$ Nanowires. *Angew. Chem., Int. Ed.* **2013**, *52*, 12332−12336.

(25) Nie, L.; Chen, M.; Sun, X.; Rong, P.; Zheng, N.; Chen, X. Palladium Nanosheets as Highly Stable and Effective Contrast Agents for in Vivo Photoacoustic Molecular Imaging. *Nanoscale* **2014**, *6*, 1271−1276.

(26) Akchurin, G.; Khlebtsov, B.; Tuchin, V.; Zharov, V.; Khlebtsov, N. Gold Nanoshell Photomodification under a Single-Nanosecond Laser Pulse Accompanied by Color-Shifting and Bubble Formation Phenomena. *Nanotechnology* **2008**, *19*, 015701.

(27) Zamiri, R.; Zakaria, A.; Husin, M.; Wahab, Z.; Nazarpour, F. Formation of Silver Microbelt Structures by Laser Irradiation of Silver Nanoparticles in Ethanol. *Int. J. Nanomed.* **2011**, *6*, 2221−2224.

(28) Yavuz, M. S.; Cheng, Y.; Chen, J.; Cobley, C. M.; Zhang, Q.; Rycenga, M.; Xie, J.; Kim, C.; Song, K. H.; Schwartz, A. G.; Wang, L. V.; Xia, Y. Gold Nanocages Covered by Smart Polymers for Controlled Release with Near-infrared Light. *Nat. Mater.* **2009**, *8*, 935−939.

(29) Tang, S.; Chen, M.; Zheng, N. Sub-10-nm Pd Nanosheets with Renal Clearance for Efficient Near-Infrared Photothermal Cancer Therapy. *Small* **2014**, DOI: 10.1002/smll.201303631.

(30) Dolmans, D.; Fukumura, D.; Jain, R. Photodynamic Therapy for Cancer. *Nat. Rev. Cancer* **2003**, *3*, 380−387.

(31) Konan, Y.; Gurny, R.; Allémann, E. State of the Art in the Delivery of Photosensitizers for Photodynamic Therapy. *J. Photochem. Photobiol. B* **2002**, *66*, 89−106.

(32) Lin, J.; Wang, S.; Huang, P.; Wang, Z.; Chen, S.; Niu, G.; Li, W.; He, J.; Cui, D.; Lu, G.; Chen, X.; Nie, Z. Photosensitizer-loaded Gold Vesicles with Strong Plasmonic Coupling Effect for Imaging-Guided Photothermal/Photodynamic Therapy. *ACS Nano* **2013**, *7*, 5320−5329.
(33) Wang, S.; Huang, P.; Nie, L.; Xing, R.; Liu, D.; Wang, Z.; Lin, J.; Chen, S.; Niu, G.; Lu, G.; Chen, X. Single Continuous Wave Laser Induced Photodynamic/Plasmonic Photothermal Therapy Using Photosensitizer-Functionalized Gold Nanostars. *Adv. Mater.* **2013**, *25*, 3055−3061.
(34) Wang, J.; Zhu, G.; You, M.; Song, E.; Shukoor, M. I.; Zhang, K.; Altman, M. B.; Chen, Y.; Zhu, Z.; Huang, C. Z.; Tan, W. Assembly of Aptamer Switch Probes and Photosensitizer on Gold Nanorods for Targeted Photothermal and Photodynamic Cancer Therapy. *ACS Nano* **2012**, *6*, 5070−5077.
(35) Jang, B.; Park, J.-Y.; Tung, C.-H.; Kim, I.-H.; Choi, Y. Gold Nanorod-Photosensitizer Complex for Near-Infrared Fluorescence Imaging and Photodynamic/PhotothermalTherapy in Vivo. *ACS Nano* **2011**, *5*, 1086−1094.
(36) Khlebtsov, B.; Panfilova, E.; Khanadeev, V.; Bibikova, O.; Terentyuk, G.; Ivanov, A.; Rumyantseva, V.; Shilov, I.; Ryabova, A.; Loshchenov, V.; Khlebtsov, N. Nanocomposites Containing Silica-coated Gold-silver Nanocages and Yb-2,4-dimethoxyhematoporphyrin: Multifunctional Capability of IR-luminescence Detection, Photosensitization, and Photothermolysis. *ACS Nano* **2011**, *5*, 7077−7089.
(37) Kuo, W.; Chang, Y.; Cho, K.; Chiu, K.; Lien, C.; Yeh, C.; Chen, S. Gold Nanomaterials Conjugated with Indocyanine Green for Dual-modality Photodynamic and Photothermal Therapy. *Biomaterials* **2012**, *33*, 3270−3278.
(38) Yu, C.; Wo, F.; Shao, Y.; Dai, X.; Chu, M. Bovine Serum Albumin Nanospheres Synchronously Encapsulating "Gold Selenium/Gold" Nanoparticles and Photosensitizer for High-efficiency Cancer Phototherapy. *Appl. Biochem. Biotechnol.* **2013**, *169*, 1566−1578.
(39) Khan, S.; Kanchanapally, R.; Fan, Z.; Beqa, L.; Singh, A.; Senapati, D.; Ray, P. A Gold Nanocage-CNT Hybrid for Targeted Imaging and Photothermal Destruction of Cancer Cells. *Chem. Commun.* **2012**, *48*, 6711−6713.
(40) Kuo, W.; Chang, C.; Chang, Y.; Yang, M.; Chien, Y.; Chen, S.; Yeh, C. Gold Nanorods in Photodynamic Therapy, as Hyperthermia Agents, and in Near-Infrared Optical Imaging. *Angew. Chem., Int. Ed.* **2010**, *49*, 2711−2715.
(41) Liao, X.; Zhang, X. Preparation, Characterization and Cytotoxicity of Carbon Nanotube-Chitosan-Phycocyanin Complex. *Nanotechnology* **2012**, *23*, 035101.
(42) Tian, B.; Wang, C.; Zhang, S.; Feng, L.; Liu, Z. Photothermally Enhanced Photodynamic Therapy Delivered by Nano-Graphene Oxide. *ACS Nano* **2011**, *5*, 7000−7009.
(43) Shi, S.; Zhu, X.; Zhao, Z.; Fang, W.; Chen, M.; Huang, Y.; Chen, X. Photothermally Enhanced Photodynamic Therapy Based on Mesoporous Pd@Ag@mSiO_2 Nanocarriers. *J. Mater. Chem. B* **2013**, *1*, 1133−1141.
(44) Peng, J.; Zhao, L.; Zhu, X.; Sun, Y.; Feng, W.; Gao, Y.; Wang, L.; Li, F. Hollow Silica Nanoparticles Loaded with Hydrophobic Phthalocyanine for Near-infrared Photodynamic and Photothermal Combination Therapy. *Biomaterials* **2013**, *34*, 7905−7912.
(45) Tada, D. B.; Vono, L. L. R.; Duarte, E. L.; Itri, R.; Kiyohara, P. K.; Baptista, M. S.; Rossi, L. M. Methylene Blue-Containing Silica-Coated Magnetic Particles: A Potential Magnetic Carrier for Photodynamic Therapy. *Langmuir* **2007**, *23*, 8194−8199.